Supplemental Data

Multiple-pinhole collimator

The second generation multiple-pinhole (MPH) collimator for brain SPECT used in the current study features a solid tungsten aperture of 18 mm thickness with 30 pinholes approximately arranged in 5 axially oriented columns and 6 transaxially oriented rows (Supplemental Figure 1). The MPH collimator was designed for targeted brain SPECT imaging with high count sensitivity and minimum multiplexing artifacts by combination of overlapping and non-overlapping projections (*1-3*) (Supplemental Figure 1, part C). More precisely, 61.5% of the detector surface are exposed to a single projection, 33.5% to 2 projections, 1% to 3 projections and 4% of the detector surface are exposed to 4 projections. As a result, the total area of the projection images is about 1.48 times larger than the detector surface.

Each pinhole is shaped like a double truncated pyramid with one rectangular pyramid base facing the patient, the other rectangular pyramid base facing the detector (Supplemental Figure 1, part A). The center of the double truncated pyramid (defining the focal plane) is located 5 mm from the outer surface of the aperture plate (facing the patient) and 13 mm from its inner surface (facing the crystal). The focus of the pinhole is a square of 4 to 5 mm edge length.

Each double truncated pinhole pyramid is sheared such that its central axis is tilted towards the patient (rather than being orthogonal to the MPH aperture plate). Therefore, the field-of-view of the MPH collimator is not centered between the MPH aperture plates, but it is shifted towards the patient (Supplemental Figure 1, part A).

The MPH aperture plate is mounted on a lead blind (Supplemental Figure 1). The inferior part of the lead blind (facing the patient) is 32 mm thick in order to efficiently shield photons originating from other parts of the body than the head. All other parts of the lead blind are 12 mm thick to limit the weight. The lead blind defines the orthogonal distance between the pinhole focal plane and the detector surface to 145 mm. For DAT-SPECT, the rotation radius should be such that the distance between the center-of-rotation axis and the face of the detector is 285 mm (the same for all patients).

SPECT acquisition with the MPH collimators is performed in step-and-shoot mode, continuous rotation mode is not available with the MPH collimators.

The total weight of one MPH collimator (aperture plate and blind) is about 100 kg. The three MPH collimators are mounted on collimator carts, one cart for two MPH collimators, another cart for the remaining MPH collimator. The same type of carts is used for conventional collimators.

Specific binding ratio analysis

The specific binding ratio (SBR) analysis used in the current study comprises three steps: (i) anatomical standardization of the individual DAT-SPECT image, (ii) intensity scaling and (iii) region-of-interest (ROI) analysis.

For anatomical standardization, the individual DAT-SPECT images were stereotactically normalized (affine, no warping) to the anatomical space of the Montreal Neurological Institute (MNI) using the Normalize tool of the Statistical Parametric Mapping software package (version SPM12) and a set of custom DAT-SPECT templates representative of normal and different levels of neurodegeneration-typical reduction of striatal uptake as target (moderate reduction more pronounced in the left hemisphere, moderate reduction more pronounced in the right hemisphere, strong bilateral reduction) (*4*). The rationale for using a set of templates including templates representative of neurodegeneration-typical reduction of striatal uptake was that using one single DAT-SPECT template representative of normal striatal [^{123}I]FP-CIT uptake might cause a bias in favor of normal DAT-SPECT images. In particular, it can cause artificial inflation and spatial shifting of striata with neurodegeneration-typical reduction of [^{123}I]FP-CIT uptake to better match healthy striata in size and localization. This results in the overestimation of reduced putaminal SBR (*4*), which might reduce the power to detect nigrostriatal degeneration by semi-quantitative analysis of DAT- SPECT. In a sample of 1702 clinical [^{123}I]FP-CIT SPECT (without overlap to the [^{123}I]FP-CIT SPECT sample of the current study), the effect size of the difference between normal and reduced putamen SBR was slightly larger with the multiple templates approach than with a the single normal template for stereotactical normalization (*4*).

For intensity scaling, each voxel in the stereotactically normalized DAT-SPECT image was divided by the individual 75th percentile of the voxel intensity in a reference region comprising the whole brain without striata, thalamus, medial temporal lobe, brainstem, cerebellum, and ventricles (*5*). A reference region mask predefined in MNI space was used for this purpose. The scaled images are semi-quantitative images representing the distribution volume ratio (DVR).

Requirements to be fulfilled by the reference region for intensity scaling in preparation of semi-quantitative analysis of [^{123}I]FP-CIT SPECT are (i) very low DAT concentration and (ii) similar non-displaceable [^{123}I]FP-CIT uptake as in the striatum. DAT density is very low in the cerebellum and all neocortical brain regions (*6*). However, there is [^{123}I]FP-CIT binding to serotonin transporters in the thalamus, medial temporal lobe and brainstem. The remainder of the brain can be assumed to fulfil these requirements to reasonable extent. Nevertheless, very often the reference region is restricted to the frontal or occipital lobe or the cerebellum. The restriction to a smaller than necessary reference region might result in increased test-retest and between-subjects variability of the SBR, not only due to increased statistical noise associated with the lower number of counts in the reference region, but also due to variability in the delineation of the reference region in each individual scan. In 70 healthy subjects from the European Normal Control Database of [^{123}I]FP-CIT, the fraction of SBR variability explained by age was higher when the whole brain (without striata) was used as reference region compared to occipital cortex and cerebellum (*7*). In 150 patients from clinical routine, whole brain (without striata, thalamus and brainstem) resulted in a higher area under the receiver operating characteristic (ROC) curve of the SBR for differentiation between neurodegenerative and non-neurodegenerative parkinsonian syndromes than occipital or frontal lobe (*5*). Whole brain without striata as reference region for [^{123}I]FP-CIT SPECT was first proposed by Livia Tossici-Bolt and co-workers (*8*).

The whole brain without striata, thalamus, medial temporal lobe, brainstem, cerebellum, and ventricles includes white matter and, in patients with strongly widened cerebrospinal fluid space (CSF), also some CSF voxels. The rationale for using the 75th percentile of the voxel intensities across this reference region was to reduce the contribution of CSF voxels. Furthermore, the 75th percentile might also account for lesions such as stroke, since even a large stroke probably alters the distribution of voxel intensities only below the 75th percentile so that the 75th percentile is not affected. In the 150 patients from clinical routine mentioned above, the 75th percentile resulted in a higher area under the ROC curve for the differentiation between neurodegenerative and non-neurodegenerative Parkinsonian syndromes compared to both, the median and the mean, independent of the reference region (whole brain without striata, occipital lobe, frontal lobe) (*5*).

Concerning the cerebellum as a reference region, in some patients (with hunched shoulders) it is difficult to achieve a small radius of rotation of the detectors if the entire cerebellum is to be included within the field-of-view. This results in the cerebellum being “cropped” in some DAT-SPECT. The rationale for excluding the cerebellum from the whole brain reference region was to avoid out of field-of-view voxels and edge effects associated with “cropping” of the cerebellum.

For the ROI analysis, hottest voxels analysis within large unilateral putamen masks predefined in MNI space was used (*9*). These masks were much bigger than the putamen in order to guarantee that the entire putamen was completely included in the mask in each individual patient, independent of some residual anatomical between-subjects variability after stereotactical normalization. The number of hottest voxels over which to average the DVR for the unilateral putamen was fixed to 10 ml (1250 cubic voxels of 2 mm edge length), which is in the range of the putamen volume of healthy subjects (*10*). In the 1702 clinical [^{123}I]FP-CIT SPECT mentioned above, the hottest voxels analysis resulted in larger effect size for the differentiation between normal and reduced DAT-SPECT than conventional ROI analysis (mean SBR in the anatomical putamen using unilateral putamen masks from the Automated Anatomical Labelling atlas) (*4,11*).

Convolutional neural network

An ensemble of 5 standard ResNet (*12*) with identical structure (Supplemental Figure 2) but different random initialization was trained for the automatic classification of the MPH-DAT-SPECT images. The network structure comprised three stages with one, one and two residual blocks and 16, 32, and 64 filters per stage. Convolution with kernel size and stride 3x3 for downsampling was used after the first and after the second block. The final residual block was followed by convolution with 1x1 kernel size, a max reduction operator and the softmax function to provide pseudo probabilities (ranging between 0 and 1) as output of the network. The cutoff 0.5 on the output was used to generate a binary decision, separately for each of the 5 networks. The majority vote across the 5 networks in the ensemble was used as final binary decison.

The 640 DAT-SPECT with 30 min scan duration were randomly split into 427 training (2/3) and 213 (1/3) test cases. The intra-reader consensus of the visual interpretation by the experienced reader was used as the gold standard label (subsection „Visual interpretation“ in „Materials and Methods“ in the manuscript). A quadratic 72x72 matrix centered at the striata was cropped from the 2-dimensional image slab of 12 mm thickness (Figure 1 in the manuscript) to serve as input to each of the 5 networks (Supplemental Figure 2). The network ensemble was trained for 60.000 batches of size twelve comprising 6 normal and 6 reduced DAT-SPECT of 30 min scan duration. A standard stochastic gradient descent optimizer with Nesterovs momentum (*13*) of factor 0.9, weight decay of magnitude 3e-5 and a learning rate schedule with a linear warmup over the first 5% of the training followed by a cosine annealing with maximum learning rate 3e-4 was used. The input images were preprocessed by clipping the intensity values at 0 and at 6.5 followed by Z-normalization using the global mean and standard deviation of intensity values in the training set (0.62 and 0.58, respectively). Excessive

data augmentation was performed including spatial methods (rotation, grid scaling, flipping), and intensity-based methods (adding of Gaussian noise, Gaussian blurring, multiplicative gray value scaling, gray value clipping, and gamma transformations) (*14*). The network ensemble was trained in a fivefold cross-validation scheme using the majority vote of the 5 networks during inference time.

Relevant loss of SBR determination

The impact of reduced scan duration on the unilateral putamen SBR was characterized by the coefficient of determination (R^2) obtained by regression analysis of the SBR from the full 30 min scan with the SBR from reduced scan duration as independent variable. The threshold on R^2 for the impact of reduced scan duration on the SBR to be "relevant" was fixed at the R^2 value that would be expected alone due to the normal variability of the putamen SBR in short-term test-retest DAT-SPECT of the same patient.

In a study on test-retest reproducibility of [^{123}I]FP-CIT SPECT, Matsuoka and co-workers performed two [^{123}I]FP-CIT SPECT in each of 8 healthy subjects (*15*). The mean time interval between the two scans was 18 ± 8 days (range 7-28 days). The variability of the SBR (in %) defined as 200*abs(test-retest)/(test+retest) was 5.7% ± 3.3%, 4.9% ± 4.2% and 7.8% ± 4.6% for striatum, caudate and putamen respectively (*15*).

The lowest of these values (5%) was used to fix the threshold on R^2 in order to be on the safe side. Computer simulations were used for this purpose. The simulations started with 1,000 noise-free SBR values uniformly distributed between 0 and 3.0 (MATLAB code: SBRnoise-free = (1:1:1000)*3/1000). Then, two noisy realizations were obtained by adding random noise, more precisely

SBRtest = (1+0.05*r1).*SBRnoise-free

and

SBRretest = (1+0.05*r2).*SBRnoise-free

where r1 and r2 are independent vectors of length 1,000 with each element randomly drawn from the standard normal distribution (".*" indicates element-wise multiplication of vectors). The coefficient of determination R^2 = 0.98 was obtained from linear regression of SBRretest versus SBRtest (Supplemental Figure 3).

Image-wise correlation

In order to identify the cases with the largest impact of the scan duration on the SPECT image, image-wise Pearson correlation coefficients were computed between the 2D slab views (used for visual interpretation, s. Figure 1 in the manuscript) with reduced scan duration and the corresponding 2D slab view from the full 30 min projection data. The MATLAB function corr2 was used for this purpose. This was done for each of the 640 DAT-SPECT and for each reduced scan duration. The results are shown in Supplemental Figure 4. Visual inspection of the cases with the lowest correlation coefficient at 12 min scan duration did not reveal any relevant differences in image quality between 12 min and 30 min scan duration that might affect the visual interpretation by less experienced readers.

Supplemental References

1. Van Audenhaege K, Vanhove C, Vandenberghe S, Van Holen R. The Evaluation of Data Completeness and Image Quality in Multiplexing Multi-Pinhole SPECT. *IEEE Trans Med Imaging*. 2015;34:474-486.

2. Lin JY. On Artifact-Free Projection Overlaps in Multi-Pinhole Tomographic Imaging. *IEEE Trans Med Imaging*. 2013;32:2215-2229.

3. Tecklenburg K, Forgacs A, Apostolova I, et al. Performance evaluation of a novel multi-pinhole collimator for dopamine transporter SPECT. *Phys Med Biol.* 2020;65.

4. Apostolova I, Schiebler T, Lange C, et al. Stereotactical normalization with multiple templates representative of normal and Parkinson-typical reduction of striatal uptake improves the discriminative power of automatic semi-quantitative analysis in dopamine transporter SPECT. *EJNMMI Phys.* 2023;10:25.

5. Kupitz D, Apostolova I, Lange C, et al. Global scaling for semi-quantitative analysis in FP-CIT SPECT. *Nuklearmedizin.* 2014;53:234-241.

6. Hall H, Halldin C, Guilloteau D, et al. Visualization of the dopamine transporter in the human brain postmortem with the new selective ligand [125I]PE2I. *Neuroimage.* 1999;9:108-116.

7. Buchert R, Kluge A, Tossici-Bolt L, et al. Reduction in camera-specific variability in [(123)I]FP-CIT SPECT outcome measures by image reconstruction optimized for multisite settings: impact on age-dependence of the specific binding ratio in the ENC-DAT database of healthy controls. *Eur J Nucl Med Mol Imaging.* 2016;43:1323-1336.

8. Tossici-Bolt L, Hoffmann SM, Kemp PM, Mehta RL, Fleming JS. Quantification of [123I]FP-CIT SPECT brain images: an accurate technique for measurement of the specific binding ratio. *Eur J Nucl Med Mol Imaging.* 2006;33:1491-1499.

9. Wenzel M, Milletari F, Krueger J, et al. Automatic classification of dopamine transporter SPECT: deep convolutional neural networks can be trained to be robust with respect to variable image characteristics. *Eur J Nucl Med Mol Imaging.* 2019;46:2800-2811.

10. Aylward EH, Li Q, Habbak QR, et al. Basal ganglia volume in adults with Down syndrome. *Psychiatry Res.* 1997;74:73-82.

11. Tzourio-Mazoyer N, Landeau B, Papathanassiou D, et al. Automated anatomical labeling of activations in SPM using a macroscopic anatomical parcellation of the MNI MRI single-subject brain. *Neuroimage.* 2002;15:273-289.

12. He K, Zhang X, Ren S, Sun J. Deep Residual Learning for Image Recognition. Paper presented at: IEEE Conference on Computer Vision and Pattern Recognition, 2016; Las Vegas, NV, USA.

13. Sutskever I, Martens J, Dahl G, Hinton G. On the importance of initialization and momentum in deep learning. Paper presented at: International Conference on Machine Learning, 2013.

14. Isensee F, Jaeger PF, Kohl SAA, Petersen J, Maier-Hein KH. nnU-Net: a self-configuring method for deep learning-based biomedical image segmentation. *Nat Methods.* 2021;18:203-211.

15. Matsuoka K, Yasuno F, Shinkai T, et al. Test-retest reproducibility of extrastriatal binding with (123)I-FP-CIT SPECT in healthy male subjects. *Psychiatry Res Neuroimaging.* 2016;258:10-15.

SUPPLEMENTAL FIGURES

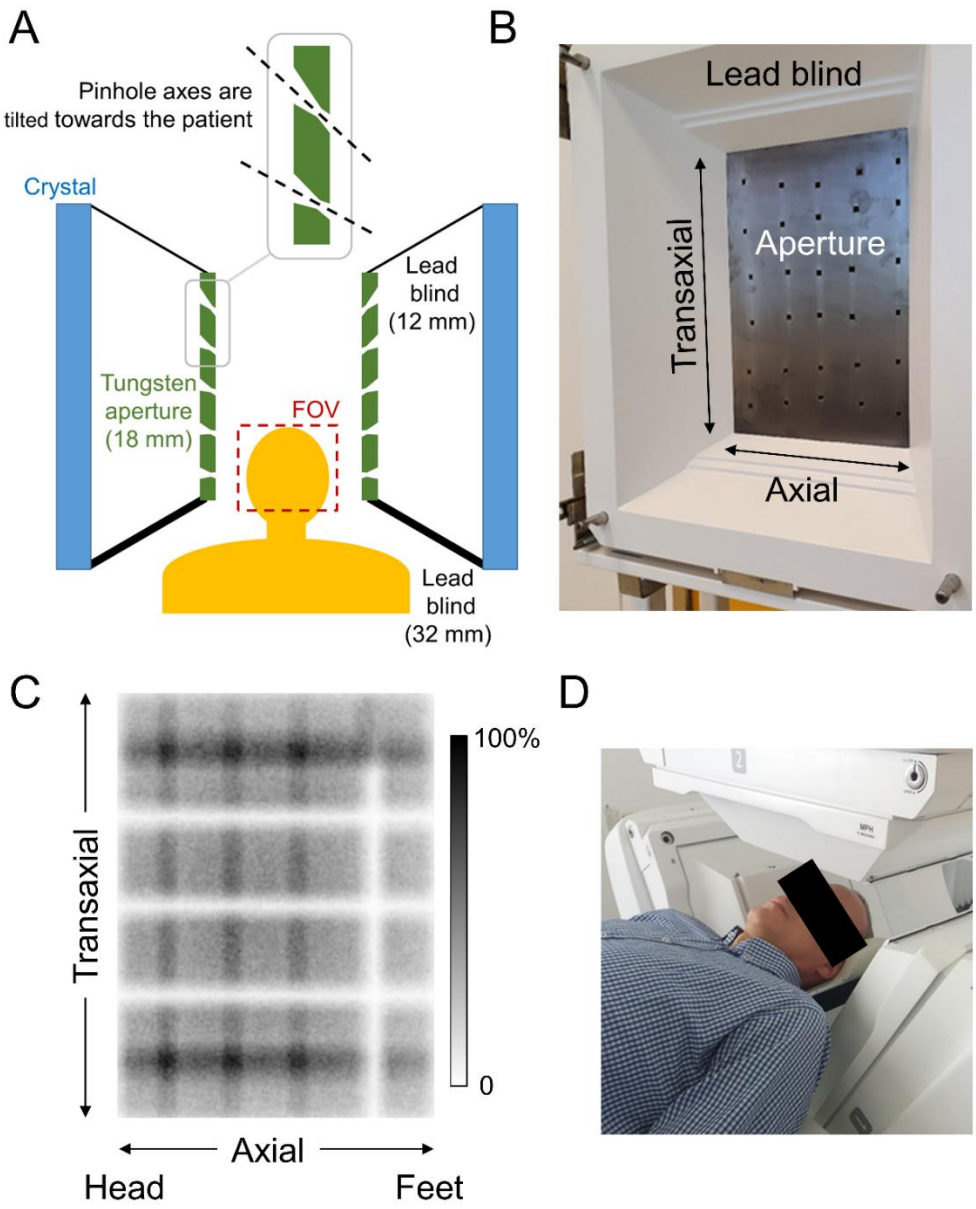

SUPPLEMENTAL FIGURE 1 (A) Drawing of the detector heads equipped with the multi-pinhole (MPH) collimator, only two of the three detector heads are shown. The pinhole axes are tilted towards the patient such that the field-of-view (FOV) is shifted towards the patient in axial direction. The drawing is not to scale. Part (B) shows a photograph of the rear view of the MPH collimator. Part (C) shows the projection pattern of a ^{57}Co flood source placed directly on the touch plate on top of the aperture. Part (D) illustrates the positioning of the patient for the SPECT acquisition.

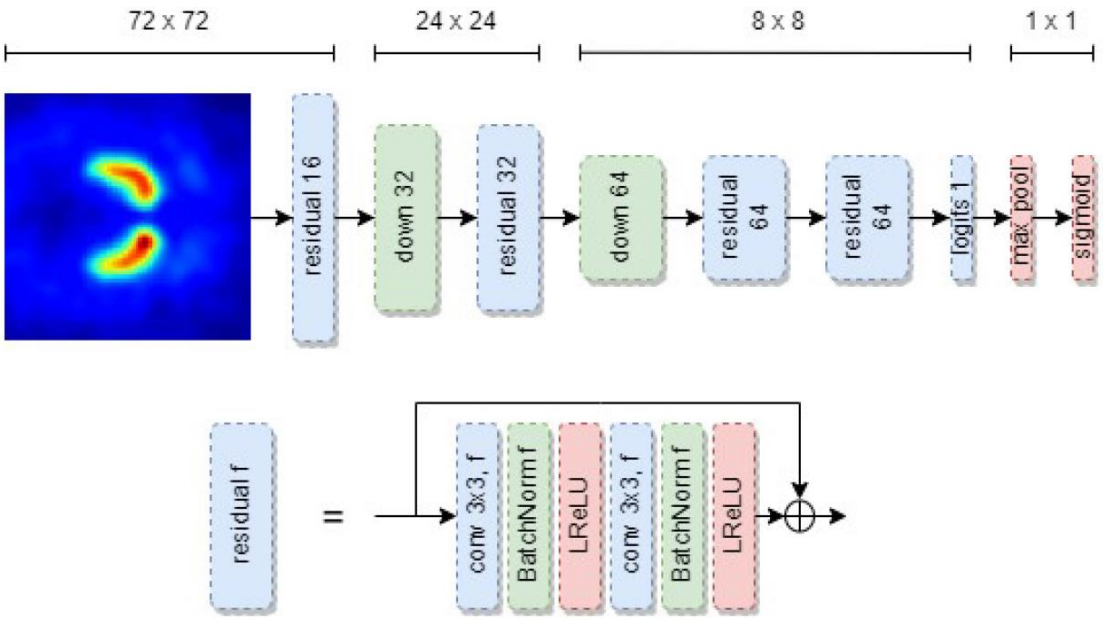

SUPPLEMENTAL FIGURE 2 ResNet with three stages trained for the automatic classification of the MPH DAT-SPECT (2-dimensional slab views) with 30 min scan duration.

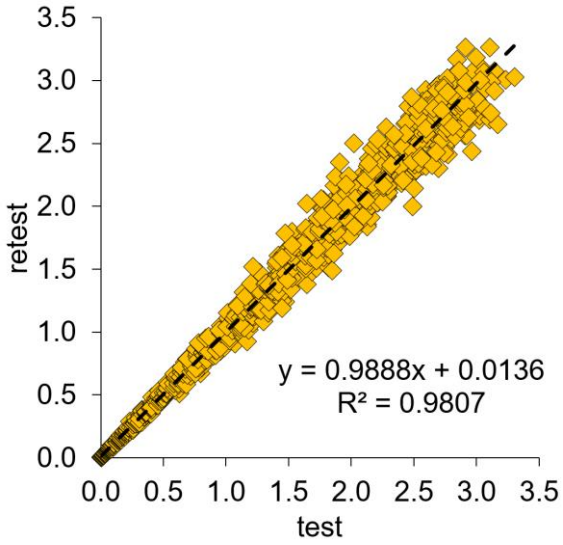

SUPPLEMENTAL FIGURE 3 Relevant loss of SBR determination: scatter plot of test and retest putamen SBR from the computer simulations assuming a relative test-retest variability of 5%.

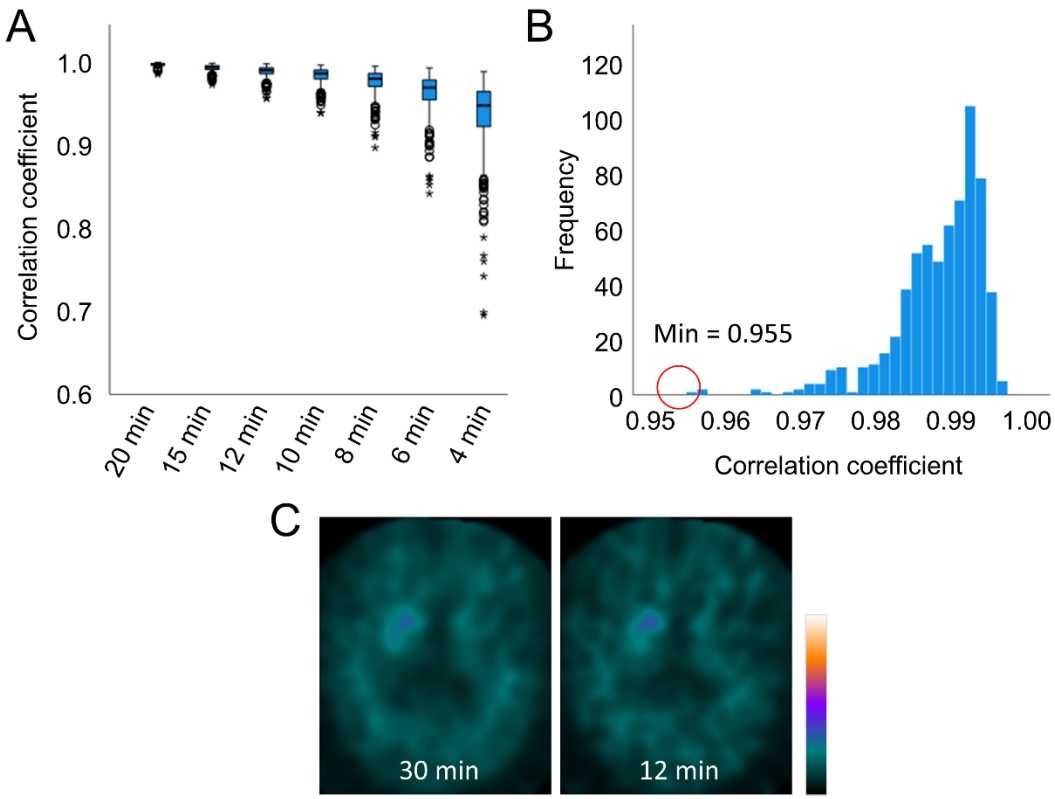

SUPPLEMENTAL FIGURE 4 A: Box and whisker plot of the Pearson correlation coefficient between the 2D slab view images with reduced scan duration and the corresponding 2D slab view image from the full 30 min projection data, **B:** histogram of the correlation coefficient at 12 min scan duration, and **C:** slab views for 30 min and 12 min scan duration for the case with the lowest correlation coefficient at 12 min scan duration (indicated by the red circle in part B).

SUPPLEMENTAL TABLES

SUPPLEMENTAL TABLE 1 Histogram analysis of the putamen SBR. Mean values M_1, M_2 and standard deviations SD_1, SD_2 from the fit of the histogram of the putamen SBR (minimum of both hemispheres, n=640) by the sum of two Gaussians according to Eq (1) in the manuscript, effect size d of the distance between the two Gaussian functions according to Eq (2), and cutoff c for the dichotomization of SBR as normal or reduced according to Eq (3). Histogram analysis was performed separately for each scan duration.

	Reduced		Normal		Effect size	Cutoff
Scan duration	M_1	SD_1	M_2	SD_2	d	c
30 min	0.475	0.209	1.741	0.382	4.116	0.923
20 min	0.492	0.195	1.723	0.371	4.157	0.916
15 min	0.512	0.198	1.737	0.356	4.254	0.951
12 min	0.542	0.212	1.762	0.352	4.201	1.000
10 min	0.563	0.212	1.776	0.345	4.243	1.025
8 min	0.597	0.226	1.803	0.343	4.151	1.076
6 min	0.635	0.224	1.821	0.338	4.139	1.107
4 min	0.720	0.238	1.894	0.430	3.381	1.139